Sphingomyelin is sorted at the *trans* Golgi network into a distinct class of secretory vesicle

Yongqiang Deng[a], Felix E. Rivera-Molina[a], Derek K. Toomre[a], and Christopher G. Burd[a,1]

[a]Department of Cell Biology, Yale School of Medicine, New Haven, CT 06520

One of the principal functions of the *trans* Golgi network (TGN) is the sorting of proteins into distinct vesicular transport carriers that mediate secretion and interorganelle trafficking. Are lipids also sorted into distinct TGN-derived carriers? The Golgi is the principal site of the synthesis of sphingomyelin (SM), an abundant sphingolipid that is transported. To address the specificity of SM transport to the plasma membrane, we engineered a natural SM-binding pore-forming toxin, equinatoxin II (Eqt), into a nontoxic reporter termed Eqt-SM and used it to monitor intracellular trafficking of SM. Using quantitative live cell imaging, we found that Eqt-SM is enriched in a subset of TGN-derived secretory vesicles that are also enriched in a glycophosphatidylinositol-anchored protein. In contrast, an integral membrane secretory protein (CD8α) is not enriched in these carriers. Our results demonstrate the sorting of native SM at the TGN and its transport to the plasma membrane by specific carriers.

sphingomyelin | Golgi apparatus | secretion | equinatoxin

Ample evidence indicates that proteins are sorted in the the *trans* Golgi network (TGN) into distinct types of Golgi-derived transport carriers (1), but little is known regarding the lipid content of different carriers. The most abundant sphingolipid, sphingomyelin (SM), is a principal component of the plasma membrane that is synthesized on the luminal membrane leaflets of TGN membranes and transported to the plasma membrane via an uncharacterized pathway. Inhibition of SM synthesis has been reported to slow Golgi-to-plasma membrane trafficking of vesicular stomatitis virus G protein, influenza hemagglutinin, and pancreatic adenocarcinoma up-regulated factor (2-6), suggesting that the SM biosynthetic pathway is broadly required for secretory competence, but the underlying mechanisms are unknown. Furthermore, it remains unclear whether SM trafficking per se, or the activities of SM metabolites such as ceramide and diacylglycerol (DAG), are harnessed for the production of secretory vesicles.

Many investigations of intracellular sphingolipid sorting use synthetic short-chain ceramides that are labeled with a fluorescent moiety that can be metabolized, albeit at slow, nonphysiological rates, to short-chain fluorescent SM and glucosylceramide (7-9). In one of the first studies of SM sorting in a polarized epithelial cell line incubated with fluorescent short-chain ceramide, fluorescently labeled lipids accumulated to a higher level in the apical membrane domain compared with the basolateral domain, suggesting that the fluorescently labeled sphingolipids are enriched in apically targeted secretory vesicles (9). A study of secretory vesicle lipid content of yeast (*Saccharomyces cerevisiae*) cells, which produce mannosylated sphingolipids (but not SM) and ergosterol (but not cholesterol), found that two types of immunopurified secretory vesicles do not differ in terms of abundances of different lipid species (10, 11). Thus, the extent to which lipid sorting occurs in the TGN remains poorly resolved, partly because of the experimental challenges of monitoring the lipid content of individual secretory vesicles. In the present study, we established an experimental approach for visualizing SM in live cells using an engineered protein that binds native SM, and implemented it to address the question of whether SM is uniformly distributed among different types of secretory vesicles.

Results and Discussion

A Genetically Encoded Probe for Sphingomyelin. The distribution of SM on the plasma membrane has been investigated with a variety of fluorescently labeled pore-forming toxins derived from marine organisms that bind directly to SM (12, 13), and we sought to construct a SM biosensor using one of these, equinatoxin II (Eqt), as a scaffold. Eqt is a member of the actinoporin family, a group of small (~20 kDa), exceptionally stable proteins that are secreted as inactive monomers and undergo conformational changes to oligomerize into a cytotoxic pore in membranes containing SM (14–20) (Fig. 1*A*). A structure of the pore formed by the homologous actinoporin fragaceatoxin C (FraC), bound to lipids (16), suggests that the pore has two SM-binding sites per protomer. Given the surface area of the pore, this stoichiometry indicates that actinoporins cannot concentrate SM above the physiological concentration of SM in Golgi membranes (21, 22). Nonetheless, two properties of native Eqt compromise its use as a SM biosensor in living cells: Eqt is cytotoxic, and although it binds specifically and with high affinity to SM, it also binds avidly to membranes that do not contain SM (23) (Fig. 1*B*).

We sought to introduce mutations into the native, mature sequence of Eqt (codons 199–735) that reduce its pore-forming activity, and thus toxicity, as well as its SM-independent membrane-binding activity. A mutation, V22W, has been shown to stabilize Eqt in a membrane-bound state before pore formation, nearly eliminating its cytolytic activity (15). In the crystal structure of the FraC pore (16), the Val22 side chain protrudes into the hydrophobic region of the membrane bilayer, consistent with the proposal that this mutation inhibits transbilayer insertion of the pore-forming helix (15). Using a liposome cosedimentation assay, we found that recombinant Eqt(V22W) retains SM recognition, and so we retained this mutation in all subsequent modifications.

Significance

The biochemical reactions that drive cellular life are housed in distinct membrane enclosed compartments known as organelles. Whereas proteins targeting to different organelles are well developed, little is known regarding how lipids are sorted to different organelles. We engineered a protein from a marine organism into a fluorescent "biosensor" of sphingomyelin (SM), a sphingolipid that is produced in the Golgi apparatus but is a major component of the plasma membrane. By monitoring SM dynamics in live cells, we discovered that SM is transported from its site of synthesis in the Golgi to the plasma membrane in a distinct type of secretory transport carrier. Our findings show that vesicle-based trafficking pathways are specialized to transport distinct types of lipids, in addition to proteins.
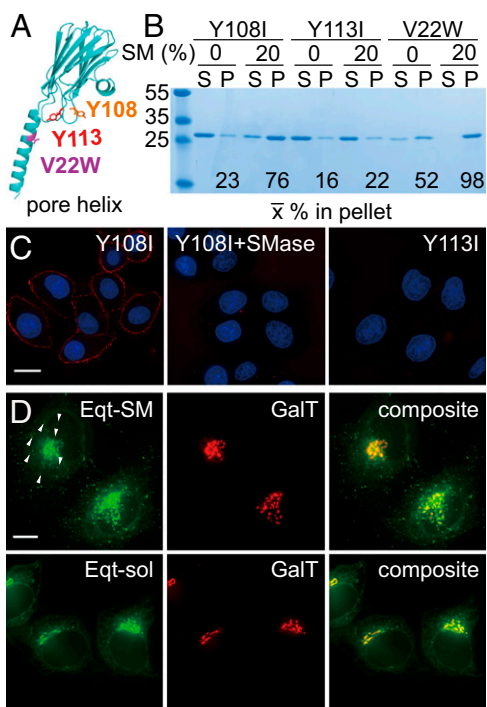
CELL BIOLOGY

Fig. 1. Membrane-binding properties and localization of Eqt derivatives. (*A*) Location of mutations introduced into Eqt. The structure of an actinoporin (FraC) protomer in its oligomeric pore-forming conformation (28) is rendered, with mutations that we introduced indicated. A residue on the N-terminal helix, V22, which was changed to tryptophan to ablate pore formation, is shown in purple. Y108, which was changed to isoleucine in Eqt-SM, is in orange, and Y113, which was changed to isoleucine in Eqt-sol, is in red. (*B*) Vesicle-binding assays. The indicated Eqt proteins were incubated with vesicles containing 20% SM or phosphatidylcholine (and 20% cholesterol), and the vesicles were collected by centrifugation. Bound pellet (P) and unbound supernatant (S) fractions were visualized by Coomassie blue staining and quantified. The mean values of three independent experiments are shown. Molecular mass standards (kDa) are indicated on the left. The Y108 and Y113 mutants also include the V22W mutation. (*C*) Eqt-V22W,Y108I recognizes SM in the plasma membrane of intact cells. Recombinant FLAG epitope-tagged Eqt-Y108I or Eqt-Y113I was incubated with HeLa cells that had been incubated with SMase or mock-treated. Cells were then washed, fixed, and incubated with anti-FLAG and labeled secondary antibodies. (*D*) Localization of Eqt-SM and Eqt-sol in HeLa cells. Plasmids encoding the indicated proteins were transfected into HeLa cells and visualized by deconvolution florescence microscopy at 16 h after transfection. The arrows point to examples of cytoplasmic puncta that contain Eqt-SM. Maximum projections of z series are shown. (Scale bar: 10 μm.)

A hydrophobic surface that is rich in aromatic residues is proposed to mediate initial membrane binding independent of SM recognition (17–20, 23, 24). Accordingly, we targeted hydrophobic residues in this region for conservative side chain substitutions and assayed the lipid-binding specificities of recombinant mutant forms of Eqt by liposome sedimentation (Fig. 1*A*). This strategy ultimately led us to identify a conservative mutation, Y108I (Eqt-V22W, Y108I), which results in a protein that binds avidly to vesicles containing 20 mole percent SM (and 60 mole percent phosphatidylcholine and 20 mole percent cholesterol), but does not bind avidly to vesicles in which phosphatidylcholine is substituted for SM (Fig. 1*B*). In contrast, a Y113I mutation (Eqt-V22W,Y113I) ablates all membrane-binding activity (Fig. 1*B*) (23). This mutant protein can serve as a control for membrane binding in future experiments. We note that the expression, solubility, and purification behavior of each mutant protein were indistinguishable from those of wild type Eqt, suggesting that these mutations do not perturb the structural integrity of the proteins.

We further examined the membrane-binding properties of purified, FLAG epitope-tagged Eqt(V22W,Y108I) and Eqt(V22W,Y113I) in a more physiological context by examining their binding to the plasma membranes of live cultured cells that had been treated with sphingomyelinase (SMase) (Fig. 1*C*). The results show that Eqt(V22W,Y108I) binds to the plasma membranes of control cells, but not to those of SMase-treated cells, and that Eqt(V22W,Y113I) does not bind to the plasma membranes of untreated or treated cells.

The effects of the Y108I and Y113I mutations can now be rationalized from crystal structures of FraC (16), along with a molecular simulation of Eqt bound to SM and phosphatidylcholine micelles (25) published after our engineering efforts were completed. SM is likely distinguished from phosphatidylcholine at two binding sites. One of these sites lies at the interface between each of the eight FraC protomers, where the bound SM molecules form part of the pore (16). The second site (termed "L2" in ref. 16) lies in the hydrophobic patch that we mutagenized. The Y113I mutation likely ablates SM recognition at this site, and also impinges on an adjacent "unspecific" (i.e., a site that does not distinguish SM) lipid-binding site (termed "L3" in ref. 16). The Y108I mutation should impinge indirectly on the unspecific L3-binding site, but not affect SM recognition at the L2 site (16, 23, 25).

Eqt-SM Is Exported from the Golgi. SM is restricted to the exofacial leaflets of cellular membranes. Thus, to visualize Eqt proteins in the secretory pathway, we replaced its native signal and pro sequences with the signal sequence of human growth hormone and fused to its C terminus the gene encoding oxGFP (26). Hereinafter, the tagged form of signal sequence-Eqt(V22W,Y108I) is referred to as "Eqt-SM," to indicate its specificity for SM, and signal sequence-Eqt(V22W,Y113I) is referred to as "Eqt-sol" to indicate that it is a soluble version of Eqt.

Plasmids containing fusion genes were cotransfected into HeLa cells with a plasmid that directs the expression of a fluorescently tagged form of β1, 4-galactosyltransferase (GalT-mKate2), a resident of the TGN (Fig. 1*D*). Anti-GFP immunoblotting showed equivalent levels of Eqt-SM and Eqt-sol when expressed in this manner. In vital dye (trypan blue) staining of transfected cultures, 16% of Eqt-V22W cells, 7% of Eqt-SM cells, 3% of Eqt-sol cells, and 2% of mock-transfected cells stained with the dye. In contrast, transfection of cells with a vector to express native Eqt (as a gene fusion similar to Eqt-SM) caused such extensive cell death that vital dye staining could not be accurately determined; the few cells that survived transfection contained numerous large vacuoles, and the GalT compartment was severely fragmented (Fig. S1*A*). These results confirm that the combination of V22 and Y108 mutations largely ablates the toxicity of Eqt-SM, and that its expression does not cause any gross alteration to Golgi morphology.

We next sought to determine whether Eqt-SM reports SM dynamics in the secretory pathway by comparing the distribution and secretion of Eqt-SM and Eqt-sol. Within the cell, Eqt-SM localized prominently to compartments decorated by GalT-mKate2 (Pearson's correlation, $R_{ave} = 0.77$) and to puncta (138 ± 47 puncta/cell) that do not contain GalT-mKate2 and are distributed throughout the cytoplasm (Fig. 1*D*, arrows). Although both Eqt-SM and Eqt-sol localized prominently to the Golgi apparatus, there were fewer cytoplasmic puncta containing Eqt-sol (18 ± 10 puncta/cell) compared with Eqt-SM (Fig. 1*D* and Table S1). Fluorescence-based colocalization studies (Fig. S2) indicated that most Eqt-SM puncta are not organelles of the endolysosomal system.

To test whether the Eqt-SM puncta are derived from the Golgi apparatus, cells were incubated at 20 °C for 3 h to block export from the TGN (27), and the appearance of Eqt-SM was determined. This incubation resulted in >10-fold depletion of Eqt-SM–containing cytoplasmic puncta (12 ± 7 puncta/cell) and accumulation of Eqt-SM in the Golgi (Fig. 2*A* and Table S1). Importantly, release of the 20 °C block by incubating the cells at 37 °C for just 30 min resulted
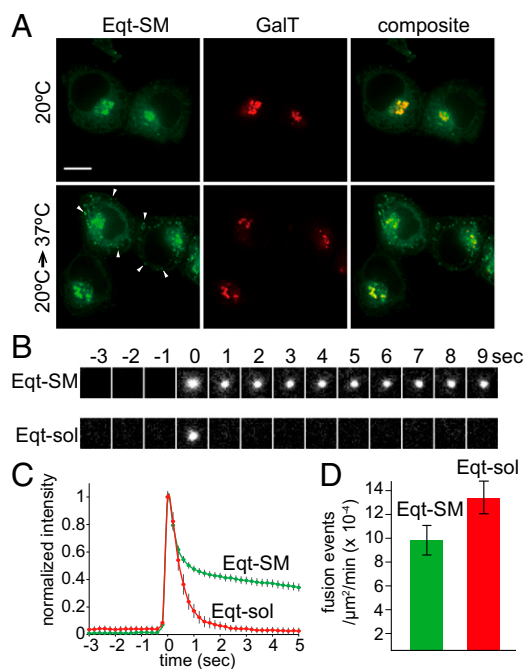
Fig. 2. Vesicles containing engineered Eqt fuse with the plasma membrane. (*A*) Blockage of export from the Golgi results in retention of Eqt-SM. HeLa cells expressing Eqt-SM (tagged with oxGFP) were incubated at 20 °C for 2 h (top row) to arrest export from the TGN and then transferred to 37 °C for 30 min. The arrows point to cytoplasmic puncta containing Eqt-SM that appeared after release of the 20 °C Golgi export block. Maximum projections of a z series are shown. (Scale bar: 10 μm.) (*B*) Representative TIRFM frames for Eqt-SM and Eqt-sol. (*C*) TIRFM showing vesicles containing Eqt-SM and Eqt-sol fused with the plasma membrane. The green and red traces indicate the average normalized fluorescence intensities for Eqt-SM (*n* = 413) and Eqt-sol (*n* = 268) vesicle fusion events, respectively (prefusion intensity defined as 0; postfusion intensity defined as 1). SDs for each point are shown. (*D*) Rates of Eqt-SM and Eqt-sol exocytic events as determined by TIRFM imaging and expressed as the number of fusion events per area (μm²) per time (min). SEMs are indicated. The rates are not statistically different ($P \leq 0.06$).

in the reappearance of Eqt-SM in cytoplasmic puncta (42 ± 22 puncta/cell), demonstrating that the Eqt-SM puncta are associated with active Golgi export (Fig. 2*A*). These results indicate that Eqt-SM is packaged into TGN-derived vesicles.

Time-lapse imaging of Eqt-SM vesicles (Movie S1) shows that they are trafficked away from the Golgi apparatus toward the cell surface. We postulated that the cytoplasmic Eqt-SM puncta are secretory vesicles, and obtained supporting evidence for this from total internal reflection fluorescence microscopy (TIRFM) imaging of Eqt-SM (Fig. 2*B* and Movie S2). For these experiments, oxGFP was replaced by the pH-sensitive fluorescent protein pHlourin (28), which allows for definitive detection of exocytic events by the flash of fluorescence occurring on exposure of pHlourin to the higher pH of the culture medium. Observation of 413 exocytic events confirmed that Eqt-SM and Eqt-sol are secreted from the cell (Fig. 2 *B* and *C*). We further confirmed that Eqt-SM-pHlourin is associated with the cell surface by demonstrating that the fluorescence signal can be quenched by the addition of trypan blue (29) to the culture medium (Fig. S1*B*). Quantitation of the average rates of exocytosis of Eqt-SM– and Eqt-sol–containing vesicles showed that Eqt-sol vesicles fuse at a faster rate than Eqt-SM vesicles (1.3×10^{-3} vs. 9.1×10^{-4} events/min, respectively; $P \leq 0.06$). Although this difference is of only modest statistical significance, it explains, at least in part, why at steady state fewer cytoplasmic Eqt-sol vesicles than Eqt-SM vesicles were observed (Fig. 1). The postfusion fluorescence decay profiles for Eqt-SM and Eqt-sol overlap for an initial phase

(∼0.5 second) but then diverge; the signal from Eqt-sol falls to baseline within 2 s owing to its diffusion away from the membrane, whereas the Eqt-SM signal persists owing to its association with the membrane. Curiously, after exocytosis, the Eqt-SM signal typically remains near the site of exocytosis (Movie S2). This may suggest that the sites of delivery and diffusion of Eqt-SM are restrained at/within the plasma membrane; however, in this study, we focused further analyses on events before fusion.

SM Synthesis Promotes Export of Eqt-SM from the Golgi. The principal site of SM synthesis is the Golgi apparatus (30-32), and inhibition of SM synthesis has been found to reduce the rate of secretion of several proteins (2-6). To examine the effect of perturbations to SM synthesis on the trafficking of Eqt-SM, we used two different methods to inhibit SM synthesis and then determined the consequences on Eqt-SM localization and secretion. First, RNA interference was used to deplete cells of the major SM synthases (SMSs), SMS1 and SMS2. The amounts of SMS1 and SMS2 mRNAs in our cultures at 2 d posttransfection were reduced by ∼70%. Our results showed a striking accumulation of Eqt-SM in the TGN and a concomitant depletion of cytoplasmic vesicles in SMS1 and SMS2 knockdown cells compared with control siRNA cells (Fig. 3*A* and Table S1).

Owing to the time required for RNAi to exert this effect, and the incomplete ablation of SMS1 and SMS2 mRNAs, we complemented this experiment with a second experiment in which SM synthesis was
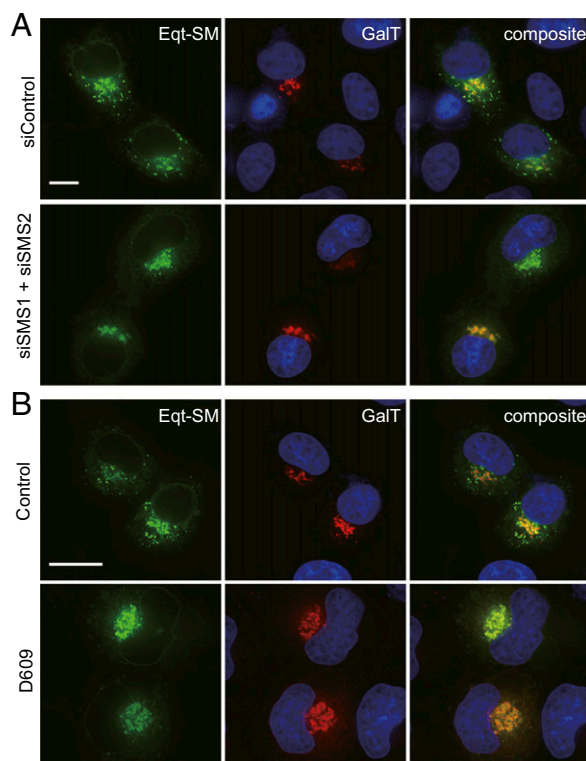

Fig. 3. Export of Eqt-SM from the Golgi is promoted by SM synthesis. (*A*) Eqt-SM accumulates in the Golgi of SMS1 and SMS2 RNAi cells. HeLa cells were transfected with siRNAs for 2 d, followed by transfected plasmids that direct expression of Eqt-SM and GalT-mKate2, and visualized by deconvolution florescence microscopy at 16 h after the second transfection. Nuclear DNA was stained with Hoechst 33342. Maximum projections of a z series are shown. (Scale bar: 10 μm.) (*B*) Eqt-SM accumulates in the Golgi of cells treated with D609, a small-molecule inhibitor of SM synthesis. HeLa cells transfected with plasmids that direct expression of Eqt-SM and GalT-mKate2 were incubated with D609 (200 μM) for 4 h. Maximum projections of a z series are shown. (Scale bar: 10 μm.)

Deng et al.

CELL BIOLOGY

acutely inhibited with D609, a small-molecule inhibitor of SM synthesis (33) and other metabolic activities (34, 35), for 4 h before imaging (Fig. 3B). Just as with SMS1 and SMS2 RNAi cells, we observed depletion of Eqt-SM cytoplasmic vesicles (14 ± 8 puncta/cell vs. 65 ± 14 puncta/cell in controls). DAG produced by the SM pathway is implicated in the fission of at least one class of Golgi-derived secretory vesicles from the TGN (36-38), but, importantly, quantitation of the proportion of a DAG sensor (PKD-C2) that localizes to the Golgi in SMS1 and SMS2 RNAi- and D609-treated cells (Fig. S3) showed no difference in SMS1 and SMS2 RNAi cells (~13% in control and RNAi cells) and just a ~50% reduction in D609-treated cells (to ~6%). These results indicate that under our experimental conditions, neither method completely eliminates the Golgi pool of DAG.

We further examined the secretory competence of D609-treated cells by monitoring the delivery of CD8α, a single-pass integral membrane protein, to the plasma membrane by fluorescence microscopy and cell surface biotinylation (Fig. S4). Our results indicate that efficient export of Eqt-SM from the Golgi requires ongoing SM synthesis, and collectively, they validate Eqt-SM as an intracellular reporter of SM trafficking. Importantly, Eqt-SM can be used to examine SM dynamics in the absence of the genetic, pharmacologic, or temperature-induced (27) perturbations commonly used in studies of post-Golgi trafficking. We took advantage of this to investigate Golgi-to-plasma membrane trafficking of native SM.

Eqt-SM Is Sorted into a Subset of Golgi-Derived Secretory Vesicles.
We performed a TIRFM-based assay of secretory vesicle content to determine whether packaging of Eqt-SM, and thus SM, is biased toward a particular class of vesicle. To ensure that the analyses were restricted to exocytic events of the biosynthetic pathway (vs., e.g., carriers derived from the endosomal pathway), fluorescent reporter proteins were retained in the endoplasmic reticulum (ER) and then released using an inducible protein aggregation system (39), which allowed us to score a biosynthetic cohort of cargo as it traversed the secretory pathway. Two different secreted cargos, a glycophosphatidylinositol (GPI) anchored protein and CD8α, were used for this. GPI was chosen because once it is delivered to the Golgi, it associates with detergent-insoluble membranes, such as those enriched in sphingolipids and cholesterol (40). The cell surface glycoprotein CD8α was chosen because, in contrast to GPI, it is excluded from detergent-insoluble membranes in T cells, where it is natively expressed (41, 42).

We constructed a GPI-anchored fusion protein containing a signal sequence, a red fluorescent protein (mKate2), and four F_M conditional aggregation domains, followed by a GPI acceptor site (ss-mKate2-FM4-GPI). This construct also contains a consensus N-glycosylation site to allow the scoring of trafficking through the Golgi using a biochemical assay (43). A structurally analogous CD8α reporter protein (ss-mKate2-FM4-CD8α) was compared with GPI (44). These constructs were introduced into HeLa cells expressing either Eqt-SM-pHlourin or Eqt-sol-pHlourin, and the cells were maintained in the absence of the disaggregation reagent ("ER retain") to restrict the residence of GPI and CD8 to the ER. On the addition of D/D solubilizer (Clontech), both reporters were released from the ER, trafficked to the Golgi apparatus, and then delivered to the plasma membrane (Fig. 4A). Exocytic events were recorded by two-color time-lapse TIRFM within 30–60 min after addition of the disaggregation reagent.

To analyze reporter protein content in each vesicle, we quantified exocytic events using two criteria. We first determined the proportions of Eqt-SM and Eqt-sol vesicles containing GPI or CD8α (Fig. 4 B and C). The results show that 72 ± 3% of Eqt-SM–containing vesicles contained GPI, whereas only 34 ± 4% of the vesicles contained Eqt-SM and CD8α (Fig. 4D). In contrast, approximately equal proportions of Eqt-sol vesicles contained GPI or CD8α (51 ± 5% and 52 ± 3%, respectively). Conversely, we calculated

the proportion of GPI-containing vesicles that contain Eqt-SM or Eqt-sol (Fig. 4D). These results show that 86 ± 5% of GPI-containing vesicles contain Eqt-SM, whereas only 51 ± 1% of these vesicles contain Eqt-sol (Fig. 4D).

The foregoing results clearly indicate a bias in the content of Eqt-SM–, and thus SM-, containing vesicles to also contain the GPI reporter, and to be de-enriched in CD8α reporter. To determine whether sorting in the Golgi apparatus underlies these biases, we released the GPI and CD8α reporters from the ER of cells expressing Eqt-SM, and then determined the proportion of GPI- or CD8α-containing vesicles that budded from the Golgi containing Eqt-SM (Fig. 5). These analyses showed that 79 ± 0.1% (n = 33) of GPI-containing carriers contained Eqt-SM, compared with only 19 ± 0.1% (n = 26) of CD8α-containing carriers. The close correspondence of these values with those of the plasma membrane fusion assays indicates that sorting of Eqt-SM, and thus of SM, and the reporter proteins occurs before exit from the Golgi apparatus. In further support of this conclusion, GPI, but not CD8α, accumulated in the Golgi of D609-treated cells after release from the ER (Fig. S4).

These results led to the prediction that GPI and CD8α are exported from the Golgi via distinct carriers. To test this, we
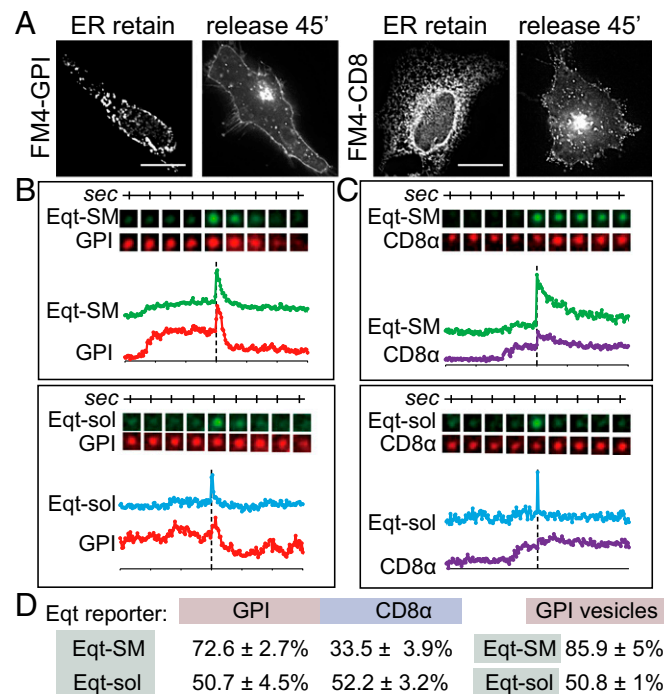

Eqt reporter:	GPI	CD8α		GPI vesicles	
Eqt-SM	72.6 ± 2.7%	33.5 ± 3.9%		Eqt-SM	85.9 ± 5%
Eqt-sol	50.7 ± 4.5%	52.2 ± 3.2%		Eqt-sol	50.8 ± 1%

Fig. 4. Eqt-SM and GPI are cosorted into secretory vesicles. (A) Trafficking of GPI and CD8α reporter proteins. HeLa cells were transfected with plasmids that direct expression of mKate2-FM4-GPI or mKate2-FM4-CD8α. In the absence of the disaggregating molecule ("ER retain") mKate2-FM4-GPI and mKate2-FM4-CD8α are retained in the ER. Incubation of cells with the disaggregating molecule ("release 45'") releases GPI and CD8α from the ER, and they are subsequently trafficked to the cell surface. The micrographs show cells incubated with solubilizer for 45 min. (B and C) Example TIRFM time-lapse gallery of Eqt-SM, Eqt-sol, and GPI (B) and mKate2-FM4-CD8α (C) exocytic events. GPI and CD8α reporters were coexpressed in cells with Eqt-SM-pHlourin or Eqt-sol-pHlourin and released from the ER of cells by the addition of solubilizer drug. Exocytic events were recorded by TIRFM beginning 30 min after ER release. The graphs show fluorescence intensity in each channel over time. (D) Summary of Eqt vesicle cargo content and GPI-containing vesicle content. The proportions of exocytic vesicles containing the indicated cargos (mean ± SD) are listed. The number of fusion events scored for each condition are as follows: Eqt-SM+CD8, n = 146; Eqt-SM+GPI, n = 157; Eqt-sol+CD8, n = 153; Eqt-sol+GPI, n = 136; GPI+Eqt-SM, n = 85; GPI+Eqt-sol, n = 65.
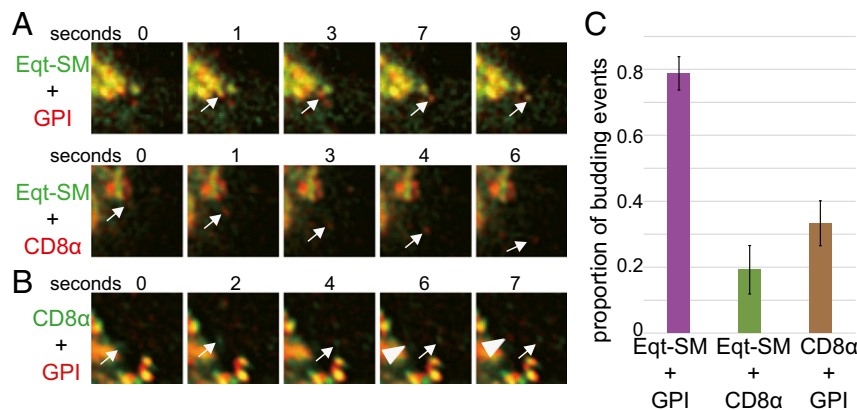
Deng et al.

Fig. 5. Eqt-SM and GPI are cosorted into vesicles that bud from the Golgi. (*A*) Time-lapse galleries showing example Golgi budding events. The fluorescent proteins (mKate2-FM4-GPI or mKate2-FM4-CD8α) were released from the ER of HeLa cells stably expressing Eqt-SM-oxGFP, and image acquisition of the Golgi region was initiated 30 min later. An example of a vesicle containing both Eqt-SM and GPI is shown at top, and an example of vesicle that contains CD8α, but not Eqt-SM, is shown below. (*B*) Time-lapse gallery of the Golgi region of a HeLa cell expressing SBP-mKate2-GPI and eGFP-FM4-CD8α, showing examples of each reporter protein being exported from the Golgi in distinct carriers. (*C*) Summary of cargo loads of vesicles that bud from the Golgi. The means ± SDs of Eqt-SM-oxGFP budding events in cells expressing mKate2-FM4-GPI (*n* = 33), mKate2-FM4-CD8α (*n* = 26), and SBP-mKate2-GPI and eGFP-FM4-CD8α (*n* = 69) are shown.

engineered cells to retain mKate2-GPI in the ER using the retention using selective hooks (RUSH) system (45) and GFP-CD8α using the aggregation-based method. Both reporters were released from the ER and arrived at the Golgi, after which the proportion of carriers that budded from the Golgi containing both proteins was determined. In close agreement with the earlier results, this analysis showed that of 69 budded carriers observed, only 33.3 ± 0.1% contained both GPI and CD8α reporters (Fig. 5).

By scoring the cargo loads of individual secretory vesicles containing an SM biosensor, Eqt-SM, as they budded from the TGN, and correlating this with the protein cargo loads of individual vesicles as they fused with the plasma membrane, we provide evidence that SM is enriched in a distinct class of secretory vesicles. The presence of Eqt-SM is strongly correlated with the presence of a secreted GPI reporter protein in the same vesicle, and anticorrelated with the presence of CD8α. Previous studies of GPI sorting and secretion in a polarized epithelial cell line were controversial (46, 47), and the results presented here firmly support the view that GPI is sorted into a distinct class of secretory vesicles that bud from the TGN (48, 49). Satisfyingly, they also support conclusions regarding the sorting of fluorescent ceramide in polarized epithelial cells (9). Nonetheless, the mechanism by which SM is selectively packaged at the TGN remains unknown. In simple membrane systems (e.g., three lipid components) at physiological temperature, SM and cholesterol coalesce into a "raft-like" liquid ordered phase (50), and lateral segregation of sphingolipid and cholesterol has been proposed to contribute to the segregation of proteins that have an intrinsic affinity for this lipid environment (51, 52). SM/cholesterol domains of sufficient size to account for secretory vesicle sorting have not been observed in the Golgi or plasma membranes, however. An alternative possibility is that spatial and temporal coupling of

SM synthesis into a "biosynthetic domain" confers a kinetic advantage for enrichment of newly synthesized SM into a distinct type of transport carrier at the TGN. The availability of Eqt-SM as a reagent to track SM in cells should provide new avenues for investigating the metabolism and trafficking of this important and abundant lipid within the cell.

Materials and Methods

DNA Manipulations. The sources of and procedures used to obtain and modify DNAs are provided in *SI Materials and Methods* (44, 45).

Cell Culture. The procedures followed to culture HeLa cells are provided in *SI Materials and Methods*.

Recombinant Protein Expression and Liposome-Binding Experiments. The purification, processing procedures, and conditions used for recombinant protein expression and liposome-binding assays are provided in *SI Materials and Methods*.

Fluorescence Microscopy. The methods and equipment used for fluorescence microscopy and image analyses are described in *SI Materials and Methods* (53, 54).

Statistical Analyses. Student's unpaired *t* test was used for statistical analyses. $P < 0.05$ was considered to indicate statistical significance.

1. De Matteis MA, Luini A (2008) Exiting the Golgi complex. *Nat Rev Mol Cell Biol* 9(4):273–284.
2. Litvak V, Dahan N, Ramachandran S, Sabanay H, Lev S (2005) Maintenance of the diacylglycerol level in the Golgi apparatus by the Nir2 protein is critical for Golgi secretory function. *Nat Cell Biol* 7(3):225–234.
3. Villani M, et al. (2008) Sphingomyelin synthases regulate production of diacylglycerol at the Golgi. *Biochem J* 414(1):31–41.
4. Subathra M, Qureshi A, Luberto C (2011) Sphingomyelin synthases regulate protein trafficking and secretion. *PLoS One* 6(9):e23644.
5. Tafesse FG, et al. (2013) Intact sphingomyelin biosynthetic pathway is essential for intracellular transport of influenza virus glycoproteins. *Proc Natl Acad Sci USA* 110(16):6406–6411.
6. Wakana Y, et al. (2015) CARTS biogenesis requires VAP-lipid transfer protein complexes functioning at the endoplasmic reticulum-Golgi interface. *Mol Biol Cell* 26(25):4686–4699.
7. Lipsky NG, Pagano RE (1983) Sphingolipid metabolism in cultured fibroblasts: Microscopic and biochemical studies employing a fluorescent ceramide analogue. *Proc Natl Acad Sci USA* 80(9):2608–2612.
8. Cooper MS, Cornell-Bell AH, Chernjavsky A, Dani JW, Smith SJ (1990) Tubulovesicular processes emerge from trans-Golgi cisternae, extend along microtubules, and interlink adjacent trans-Golgi elements into a reticulum. *Cell* 61(1):135–145.
9. van Meer G, Stelzer EH, Wijnaendts-van-Resandt RW, Simons K (1987) Sorting of sphingolipids in epithelial (Madin-Darby canine kidney) cells. *J Cell Biol* 105(4):1623–1635.

CELL BIOLOGY

Deng et al.

10. Klemm RW, et al. (2009) Segregation of sphingolipids and sterols during formation of secretory vesicles at the trans-Golgi network. *J Cell Biol* 185(4):601–612.
11. Surma MA, Klose C, Klemm RW, Ejsing CS, Simons K (2011) Generic sorting of raft lipids into secretory vesicles in yeast. *Traffic* 12(9):1139–1147.
12. Makino A, et al. (2015) Visualization of the heterogeneous membrane distribution of sphingomyelin associated with cytokinesis, cell polarity, and sphingolipidosis. *FASEB J* 29(2):477–493.
13. Abe M, Kobayashi T (2014) Imaging local sphingomyelin-rich domains in the plasma membrane using specific probes and advanced microscopy. *Biochim Biophys Acta* 1841(5):720–726.
14. Kristan KC, Viero G, Dalla Serra M, Macek P, Anderluh G (2009) Molecular mechanism of pore formation by actinoporins. *Toxicon* 54(8):1125–1134.
15. Gutiérrez-Aguirre I, et al. (2004) Membrane insertion of the N-terminal alpha-helix of equinatoxin II, a sea anemone cytolytic toxin. *Biochem J* 384(Pt 2):421–428.
16. Tanaka K, Caaveiro JM, Morante K, González-Mañas JM, Tsumoto K (2015) Structural basis for self-assembly of a cytolytic pore lined by protein and lipid. *Nat Commun* 6:6337.
17. Rojko N, et al. (2013) Membrane damage by an α-helical pore-forming protein, Equinatoxin II, proceeds through a succession of ordered steps. *J Biol Chem* 288(33):23704–23715.
18. Hong Q, et al. (2002) Two-step membrane binding by Equinatoxin II, a pore-forming toxin from the sea anemone, involves an exposed aromatic cluster and a flexible helix. *J Biol Chem* 277(44):41916–41924.
19. Athanasiadis A, Anderluh G, Macek P, Turk D (2001) Crystal structure of the soluble form of equinatoxin II, a pore-forming toxin from the sea anemone *Actinia equina*. *Structure* 9(4):341–346.
20. Anderluh G, et al. (2005) Interaction of the eukaryotic pore-forming cytolysin equinatoxin II with model membranes: 19F NMR studies. *J Mol Biol* 347(1):27–39.
21. Keenan TW, Morré DJ (1970) Phospholipid class and fatty acid composition of Golgi apparatus isolated from rat liver and comparison with other cell fractions. *Biochemistry* 9(1):19–25.
22. van Meer G, Voelker DR, Feigenson GW (2008) Membrane lipids: Where they are and how they behave. *Nat Rev Mol Cell Biol* 9(2):112–124.
23. Bakrac B, et al. (2008) Molecular determinants of sphingomyelin specificity of a eukaryotic pore-forming toxin. *J Biol Chem* 283(27):18665–18677.
24. Mancheño JM, Martín-Benito J, Martínez-Ripoll M, Gavilanes JG, Hermoso JA (2003) Crystal and electron microscopy structures of sticholysin II actinoporin reveal insights into the mechanism of membrane pore formation. *Structure* 11(11):1319–1328.
25. Weber DK, et al. (2015) Characterization of the lipid-binding site of Equinatoxin II by NMR and molecular dynamics simulation. *Biophys J* 108(8):1987–1996.
26. Costantini LM, et al. (2015) A palette of fluorescent proteins optimized for diverse cellular environments. *Nat Commun* 6:7670.
27. Matlin KS, Simons K (1983) Reduced temperature prevents transfer of a membrane glycoprotein to the cell surface but does not prevent terminal glycosylation. *Cell* 34(1):233–243.
28. Miesenböck G, De Angelis DA, Rothman JE (1998) Visualizing secretion and synaptic transmission with pH-sensitive green fluorescent proteins. *Nature* 394(6689):192–195.
29. Vranic S, et al. (2013) Deciphering the mechanisms of cellular uptake of engineered nanoparticles by accurate evaluation of internalization using imaging flow cytometry. *Part Fibre Toxicol* 10:2.
30. Tafesse FG, et al. (2007) Both sphingomyelin synthases SMS1 and SMS2 are required for sphingomyelin homeostasis and growth in human HeLa cells. *J Biol Chem* 282(24):17537–17547.
31. Lee NP, Mruk DD, Xia W, Cheng CY (2007) Cellular localization of sphingomyelin synthase 2 in the seminiferous epithelium of adult rat testes. *J Endocrinol* 192(1):17–32.
32. Ding T, et al. (2008) SMS overexpression and knockdown: Impact on cellular sphingomyelin and diacylglycerol metabolism, and cell apoptosis. *J Lipid Res* 49(2):376–385.
33. Luberto C, Hannun YA (1998) Sphingomyelin synthase, a potential regulator of intracellular levels of ceramide and diacylglycerol during SV40 transformation: Does sphingomyelin synthase account for the putative phosphatidylcholine-specific phospholipase C? *J Biol Chem* 273(23):14550–14559.
34. Amtmann E (1996) The antiviral, antitumoural xanthate D609 is a competitive inhibitor of phosphatidylcholine-specific phospholipase C. *Drugs Exp Clin Res* 22(6):287–294.
35. Adibhatla RM, Hatcher JF, Gusain A (2012) Tricyclodecan-9-yl-xanthogenate (D609) mechanism of actions: A mini-review of literature. *Neurochem Res* 37(4):671–679.
36. Liljedahl M, et al. (2001) Protein kinase D regulates the fission of cell surface destined transport carriers from the trans-Golgi network. *Cell* 104(3):409–420.
37. Baron CL, Malhotra V (2002) Role of diacylglycerol in PKD recruitment to the TGN and protein transport to the plasma membrane. *Science* 295(5553):325–328.
38. Campelo F, Malhotra V (2012) Membrane fission: The biogenesis of transport carriers. *Annu Rev Biochem* 81:407–427.
39. Rivera VM, et al. (2000) Regulation of protein secretion through controlled aggregation in the endoplasmic reticulum. *Science* 287(5454):826–830.
40. Brown DA, Rose JK (1992) Sorting of GPI-anchored proteins to glycolipid-enriched membrane subdomains during transport to the apical cell surface. *Cell* 68(3):533–544.
41. Arcaro A, et al. (2001) CD8beta endows CD8 with efficient coreceptor function by coupling T cell receptor/CD3 to raft-associated CD8/p56(lck) complexes. *J Exp Med* 194(10):1485–1495.
42. Pang DJ, Hayday AC, Bijlmakers MJ (2007) CD8 Raft localization is induced by its assembly into CD8alpha beta heterodimers, not CD8alpha alpha homodimers. *J Biol Chem* 282(18):13884–13894.
43. Keller P, Toomre D, Díaz E, White J, Simons K (2001) Multicolour imaging of post-Golgi sorting and trafficking in live cells. *Nat Cell Biol* 3(2):140–149.
44. Lavieu G, Zheng H, Rothman JE (2013) Stapled Golgi cisternae remain in place as cargo passes through the stack. *eLife* 2:e00558.
45. Boncompain G, et al. (2012) Synchronization of secretory protein traffic in populations of cells. *Nat Methods* 9(5):493–498.
46. Polishchuk R, Di Pentima A, Lippincott-Schwartz J (2004) Delivery of raft-associated, GPI-anchored proteins to the apical surface of polarized MDCK cells by a transcytotic pathway. *Nat Cell Biol* 6(4):297–307.
47. Schuck S, Simons K (2006) Controversy fuels trafficking of GPI-anchored proteins. *J Cell Biol* 172(7):963–965.
48. Paladino S, Pocard T, Catino MA, Zurzolo C (2006) GPI-anchored proteins are directly targeted to the apical surface in fully polarized MDCK cells. *J Cell Biol* 172(7):1023–1034.
49. Hua W, Sheff D, Toomre D, Mellman I (2006) Vectorial insertion of apical and basolateral membrane proteins in polarized epithelial cells revealed by quantitative 3D live cell imaging. *J Cell Biol* 172(7):1035–1044.
50. Sankaram MB, Thompson TE (1990) Interaction of cholesterol with various glycerophospholipids and sphingomyelin. *Biochemistry* 29(47):10670–10675.
51. Simons K, van Meer G (1988) Lipid sorting in epithelial cells. *Biochemistry* 27(17):6197–6202.
52. Simons K, Ikonen E (1997) Functional rafts in cell membranes. *Nature* 387(6633):569–572.
53. Rivera-Molina F, Toomre D (2013) Live-cell imaging of exocyst links its spatiotemporal dynamics to various stages of vesicle fusion. *J Cell Biol* 201(5):673–680.
54. Xu Y, et al. (2011) Dual-mode of insulin action controls GLUT4 vesicle exocytosis. *J Cell Biol* 193(4):643–653.

Deng et al.

www.manaraa.com